ELSEVIER

Journal of Nuclear Materials 270 (1999) 194–211

journal of nuclear materials

Current knowledge on core degradation phenomena, a review

P. Hofmann *

Forschungszentrum Karlsruhe, Institut für Materialforschung I, Postfach 3640, 76021 Karlsruhe, Germany

Received 21 May 1998; accepted 16 November 1998

Abstract

Degraded core processes are a key factor in the progression of a severe accident; they provide the initial conditions for in- and ex-vessel phenomena, lead to threats to the containment and determine the fission product and hydrogen source term. The knowledge of in-vessel melt relocation processes is also important with respect to cooling recovery actions (flooding of the core) and reactor pressure vessel (RPV) failure analysis. The core-melt progression is a non-coherent stepwise process which results in melting and liquefaction of core materials at different temperatures; oxidized Zircaloy cladding shells may significantly delay or prevent relocation of molten (U, Zr, O) mixtures contained within them. The various melts solidify on cooldown at different temperatures, i.e. at different axial locations, with ceramic crusts overlying metallic ones. These crusts may support melt pools; if the accident is unrecovered, the crusts may fail leading to massive relocation of molten material and debris into the lower plenum. Reflooding of an overheated core can result in a renewed temperature rise with localized melt formation, additional release of fission products, and in an increased hydrogen production; this increases the threat to the integrity of the reactor pressure vessel and to the containment as well as potentially misleading the operators regarding their recovery actions. There are principal remaining technical uncertainties in predicting late-phase core degradation after the initial intact rod geometry has been lost and regarding the effects of irradiated fuel which still have to be examined. © 1999 Elsevier Science B.V. All rights reserved.

1. Introduction

A joint European research program on 'Core Degradation' has been performed, which has been sponsored by the Commission of the European Communities [1,2]. The objective has been to improve the understanding and analytical description of in-vessel degraded core phenomena in a LWR through experimental and modeling studies.

This paper describes the current status of knowledge concerning in-vessel degraded core phenomena and their consequences on core damage progression, melt formation and material relocation processes in severe LWR accidents. It also describes the principal remaining uncertainties which have to be resolved to improve safety assessments.

The experimental results obtained on high-temperature core material behavior will provide the data base for the development of more accurate analytical models [3]. The implementation of the models in existing code systems should improve predictions of the time- and temperature-dependent core degradation processes.

2. Accident conditions

Severe accidents may result from failure of systems designed to cope with accidents. For example, a small leak in the cooling system of the primary circuit, along with a temporary failure of the emergency cooling system, may lead to core uncovery. The continuous heat-up of the core by the decay heat of the fission products can cause substantial damage up to complete meltdown of the core in unmitigated accident sequences.

With respect to core-melt progression, it is important to understand and to describe:

- how a severe accident progresses,

* Tel.: +49-7247 82 2517; fax: +49-7247 82 4567; e-mail: peter.hofmann@imf.fzk.de.

0022-3115/99/$ – see front matter © 1999 Elsevier Science B.V. All rights reserved.
PII: S0022-3115(98)00899-X

- how to mitigate its consequences, and
- how to terminate it.

A central issue in addressing these questions is the investigation of the physico-chemical behavior of the reactor core during a severe accident:

- when and how the core loses is original geometry,
- what configurations are formed,
- how much hydrogen is generated by steam oxidation of core materials,
- what influence of core degradation exists on the release of fission products (source term),
- by what processes solid and liquid core materials are transported within the core and to the lower plenum of the reactor pressure vessel,
- coolability of partially blocked cores, fuel debris beds, molten pools,
- mechanism, threshold and location of the melt-through of the ceramic melt pool,
- pathway and mode (gradual, coherent) of melt relocations under 'wet-core' and 'dry-core' conditions, and
- influence of flooding (quenching) of degraded cores on the hydrogen source term.

A better understanding of in-vessel degraded core phenomena is important for

- the purposes of accident management measures,
- risk assessments, and
- the design of safety-improved reactors of the next generation.

In general, in-vessel core melt progression provides an important input for all reactor pressure vessel and containment failure issues. For example, the quantity, temperature, physical and chemical composition, release rate, and pressure of the melt released from the reactor pressure vessel, the amount of hydrogen generated and steam available can all affect the integrity of the containment and thus have an impact on the risk [1].

3. Degraded core accident progression

A severe accident sequence involves a large number of phenomena that can be extended over long periods of time. The importance of any particular phenomenon will change as the accident progresses. The time from accident initiation up to core uncovery varies from very short times of less than 10 min to very long times of about 6–10 h. Also the system pressure varies between about 0.3 and 15 MPa during transients without depressurization. After the core is uncovered the mixture level is established in the lower core region ('wet' core), or in case of BWR below the core ('dry' core). The low mixture level results in very low steam generation and steam flow into the core. The reduced heat transfer from the fuel to the steam is low compared with decay heat, and the fuel temperatures increase. The heat-up phase extends up to the point where stability limits of some materials in the core structure are reached, complex chemical reactions are involved, melting and liquefaction occurs and the accident proceeds through the core melt and relocation phase.

The temperature transient of the core during the heat-up phase drives other different phenomena which, in turn, may influence later core melt progression in a crucial fashion. Oxidation of Zircaloy cladding materials by steam becomes a significant heat source which increases with temperature; if the heat removal capability is lost, it determines a feedback between temperature increase and cladding oxidation. Relocation of molten (hot) material into cooler core regions may initiate temperature escalation there. To predict the material behavior in severe reactor accidents, a quantitative description of the different interrelated material interactions as functions of temperature and time is needed.

The in-vessel core-melt progression should be divided in so-called unmitigated and mitigated degraded core accidents. A few of the material relocation processes will be different or can even be avoided in mitigated accident scenarios. However, since this depends strongly on the individual accident sequence a more general description of the physico-chemical material behavior in the core with increasing temperature will be given (Fig. 1) [4]:

- plastic deformation and bursting or collapsing of the cladding, depending on the differential pressure during a low- or high-pressure accident scenario,
- melting of the Ag–In–Cd absorber alloy and, after failure of the stainless steel cladding, chemical interactions with Zircaloy guide and cladding tubes in PWRs,
- eutectic interactions between boron carbide (B_4C) and stainless steel, Zircaloy–Inconel, and Zircaloy/stainless steel in BWRs, VVERs and some PWRs,
- oxidation and embrittlement of the Zircaloy cladding by steam and UO_2, which may result in rod fragmentation,
- oxidation of the stainless steel and Inconel by steam,
- melting of stainless steel and Inconel,
- oxidation of B_4C by steam,
- melting of the metallic Zircaloy cladding or the metallic oxygen-stabilized α-Zircaloy (α-Zr(O) phase),
- localized, limited oxidation of the fuel by steam in steam-rich core regions,
- reduction of the UO_2 fuel due to interactions with solid and/or molten metallic Zircaloy, with partial dissolution and disintegration of UO_2, forming a metallic Zr–U–O melt, which may contain ceramic (U, Zr)O_{2-x} precipitations at higher oxygen concentrations,
- formation of an α-Zr(O)–zirconium dioxide (ZrO_2) eutectic,
- melting of B_4C,

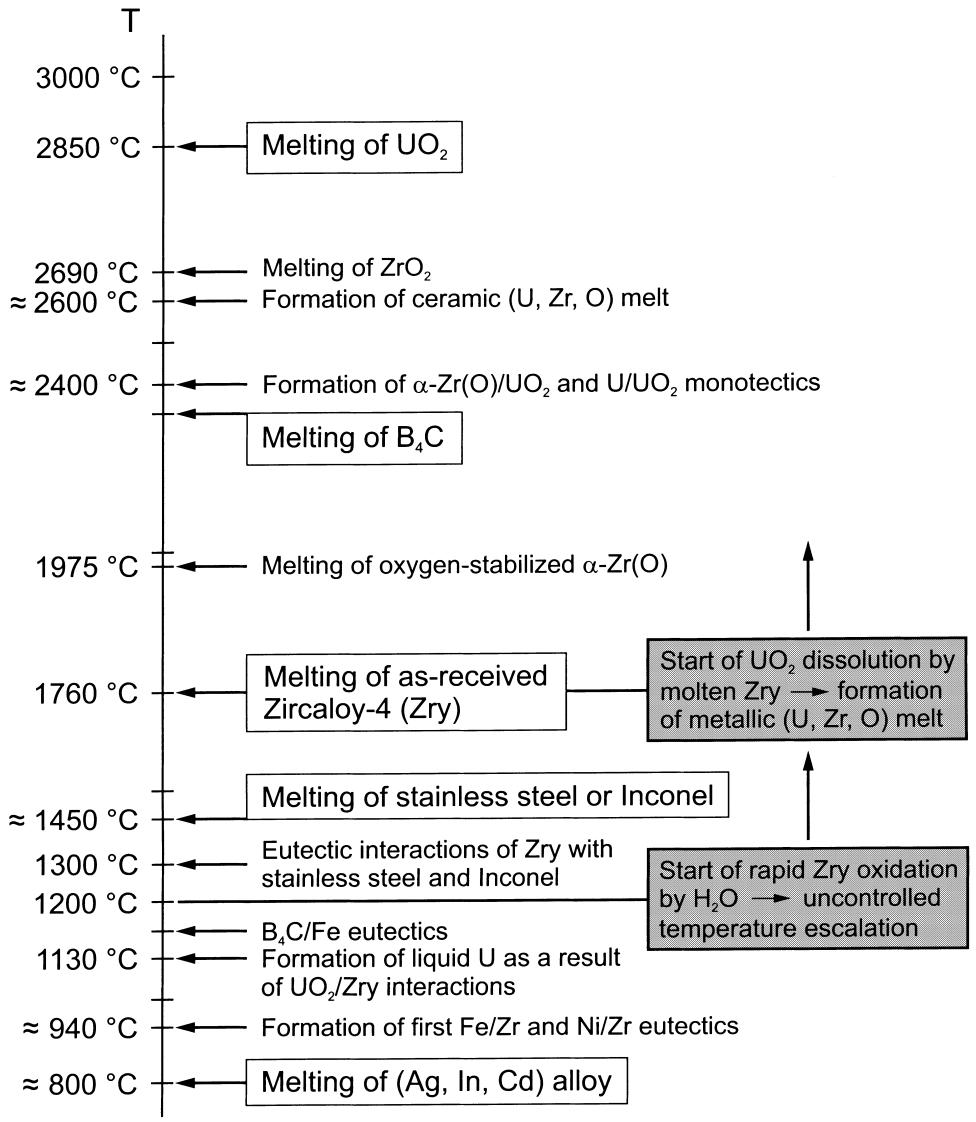

Fig. 1. LWR severe accident-relevant melting and chemical interaction temperatures which result in the formation of liquid phases.

- eutectic and monotectic reactions between α-Zr(O) and UO_2,
- melting of ZrO_2 and UO_2 forming a ceramic Zr–U–O melt,
- formation of immiscible metallic and ceramic melts in different parts of the reactor core,
- relocation of the solid and liquid materials into the lower reactor pressure vessel (RPV) head, and
- thermal, mechanical and chemical attack of the RPV wall.

At temperatures above 1200°C the rapid oxidation of Zircaloy and of stainless steel by steam results in local uncontrolled temperature escalations within the core with peak temperatures >2000°C. As soon as the Zircaloy cladding starts to melt (>1760°C), the solid UO_2 fuel may be chemically dissolved and thus liquefied about 1000 K below its melting point. As a result, liquefied fuel relocations can already take place at about 2000°C.

Many of these physical and chemical processes have been identified in separate-effects tests, out-of-pile and in-pile integral severe fuel damage (SFD) experiments, and Three Mile Island Unit 2 (TMI-2) core material examinations [5–10,33]. All of these interactions are of concern in a severe accident, because relocation and/or solidification of the resulting fragments or melts may result in local cooling channel blockages of different sizes and may cause further heatup of these core regions

because cooling still can be inadequate, causing further melt progression and material relocations into lower regions of the RPV.

Another phenomenon is the formation of rubble beds. The collapse of solid material onto the blockages (solidified materials and grid spacers) can form debris beds on top of the blockages. Continuous heatup of these debris beds can form molten pools, held in place by a solid crust, which acts as a crucible (as evidenced by TMI-2 [8]), with later crust collapse possibly influencing the late melt relocation stage.

The liquid phases are formed at different temperatures during in-vessel core melt progression; they are formed in a complex pattern involving both spatial and temporal variations. As a result, the melt progression begins at different times at different places in the core. The various molten phases will solidify on cooldown at different temperatures and will therefore form blockages at different axial locations. All these processes have a strong influence on hydrogen generation, natural circulation, the chemical composition of the melt in the lower RPV head, and its temperatures. For this reason, the material relocation processes have to be modeled and considered as precisely as possible in the code systems.

The presence of water and/or the injection of water due to safety devices or operator interactions have an important effect on the in-vessel core-melt progression. For example, if emergency core cooling water enters the reactor vessel early during the melt-down process (early reflood), there will be only limited fragmentation and collapse of solid but embrittled material. The longer the delay is in establishing this water flow (late reflood), the more there will be of both molten and embrittled materials. Ultimately, in-core configurations could be formed by this water flow that are not coolable in place. This is thought to have caused the collapse of molten material into the RPV lower head in TMI-2. During the process of melt relocation the grid structures can provide a major impediment to the downward movement of melts.

4. Chemical interactions between the various core materials

4.1. UO_2 fuel/Zircaloy cladding interactions

Besides oxidation of the cladding from the outside by steam, oxidation of the cladding from the inside by UO_2 fuel occurs, especially at higher temperatures.

The results of the UO_2 fuel/solid Zircaloy reaction experiments under isothermal and transient temperature conditions were extensively described in Refs. [11,12]. The results show that, due to oxygen uptake by the Zircaloy cladding from reaction with gaseous oxygen or steam on the outside and from reaction with UO_2 on the inside, oxygen-stabilized α-Zr(O) phases, ZrO_2, and a metallic U–Zr alloy form. The sequence of the various phases or reaction layers, starting from the inside surface, for isothermal and transient temperature experiments at all temperatures examined (800–1700°C) is

$$(UO_2+U) \rightarrow (\alpha\text{-}Zr(O)_a + (U,Zr)) \rightarrow (U,Zr)\,\text{alloy}, \rightarrow \alpha\text{-}Zr(O)_b \rightarrow \beta\text{-Zircaloy}, \rightarrow \alpha\text{-}Zr(O)_c \rightarrow ZrO_2.$$

Fig. 2 shows the sequence of the external and internal interaction layers. The U–Zr alloy within the α-$Zr(O)_a$ layer is concentrated mainly at the grain boundaries, but also exists within the matrix. The α-$Zr(O)_{a,b}$ layers forming on the inside of the cladding and the α-$Zr(O)_c$ layer forming on the outside of the cladding grow at roughly the same rates. Moreover, due to the elevated oxygen potential (oxygen partial pressure) of the gas mixture or steam compared to stoichiometric UO_2, a ZrO_2 layer also forms on the external cladding surface. Initially, the growth of the reaction layers obeys parabolic rate laws. However, because the wall thickness of the cladding is small (typically 0.57–0.72 mm), the tubing must be considered as a finite system. Therefore, the external and internal oxygen uptakes influence each other and an accelerated growth of the reaction layers is observed at longer reaction times, especially after the β-Zircaloy phase has disappeared.

With increasing time, the β-phase of the cladding disappears due to oxygen uptake and transformation into α-Zr(O). After the disappearance of the β-Zircaloy phase, the oxidized cladding tube is completely embrittled and is no longer mechanically stable. The slightest force exerted during cooling, quenching, or subsequent handling causes the fuel rod sections to break apart. Because embrittlement of the cladding occurs as a result of the formation of oxygen-stabilized α-Zr(O), the internal oxidation makes approximately the same contribution as the external oxidation. Therefore, embrittlement of the cladding occurs about four times faster than by single-sided oxidation alone. Further oxidation of the cladding results in a complete transformation of the α-Zr(O) into ZrO_2.

A comparison of the parabolic growth rate equations of the entire reaction zones for the UO_2/Zircaloy, O_2/Zircaloy, and H_2O/Zircaloy chemical interactions is shown in Fig. 3. Note that the total UO_2/Zircaloy growth rate curve overlaps the steam/Zircaloy region (result of six investigations [11] above $\approx$1100°C). This means that the UO_2/Zircaloy reaction occurs as rapidly as the steam/Zircaloy reaction above $\approx$1100°C. The change in slope of the O_2/Zircaloy reaction curve at 1100°C does not indicate a change in the reaction mechanism; it only reflects the best fit of the experimental data.

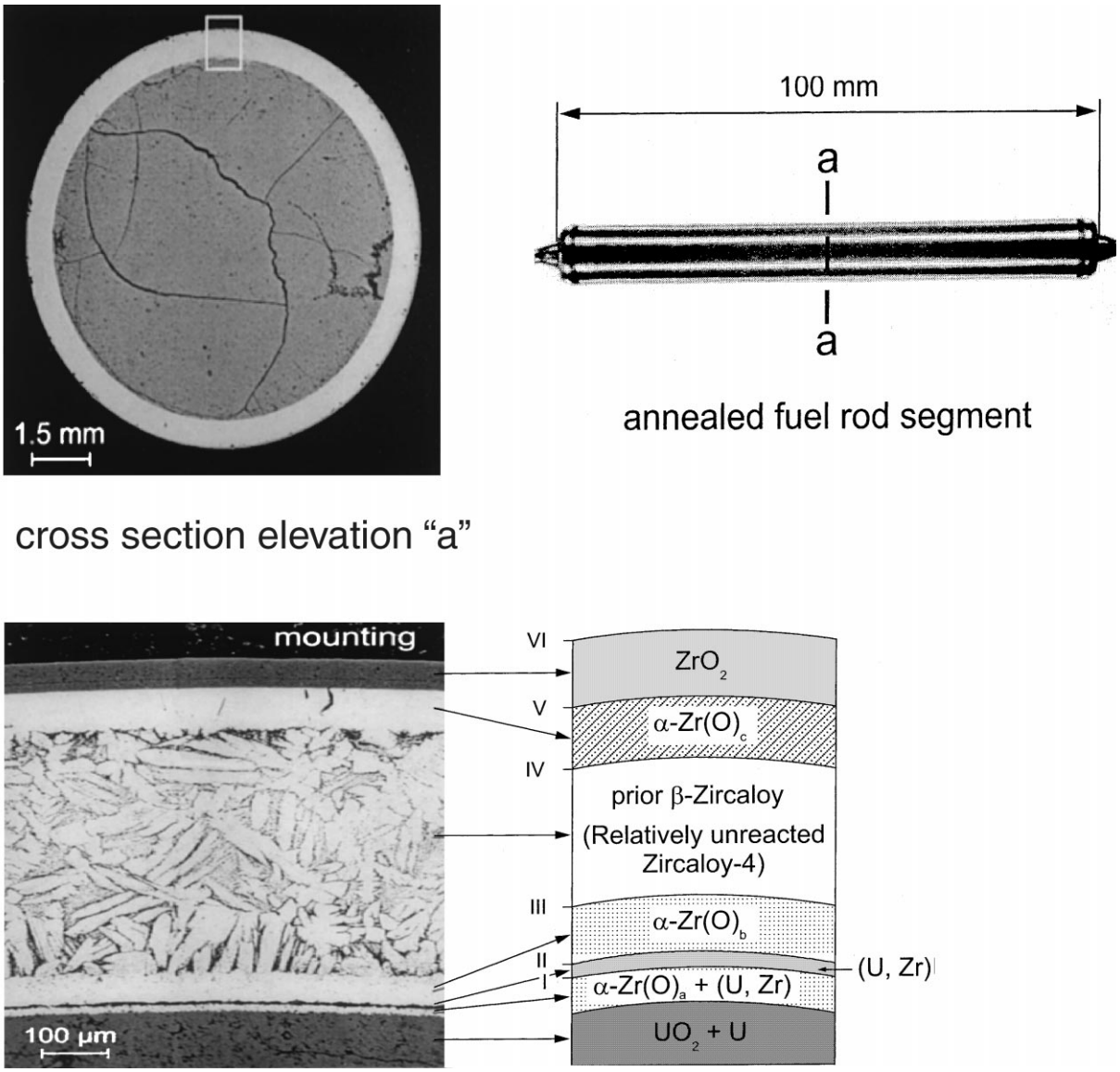

Fig. 2. Sequence of external oxygen/Zircaloy and internal UO_2/Zircaloy interaction layers in fuel rod cladding tube at 1200°C after 180 s.

The modeling of the combined internal and external cladding interactions resulted in the PECLOX numerical model, which solves the Fick and Stefan equations. It predicts the formation, growth, and disappearance of the various interaction layers and the corresponding oxygen profiles as a function of temperature and time up to complete Zircaloy cladding oxidation [13]. In this respect, the PECLOX model has major advantages over other models [12], which attempt only to simulate the kinetics of the system in the first stages of the process, when all interface movements obey parabolic rate laws (infinite systems).

4.2. UO_2 dissolution by molten Zircaloy

The meltdown behavior of Zircaloy cladding depends decisively on the extent of the cladding oxidation and on the possible formation of a ZrO_2 oxide layer during the heating period. However, the oxygen uptake by Zircaloy depends not only on the oxygen potential of the environment, but also on the chemical interaction with the UO_2 fuel, which is determined by the fuel/cladding contact conditions, i.e., the external overpressure [11]. Under oxidizing conditions, an oxide layer forms on the outer cladding surface during heating before the melting

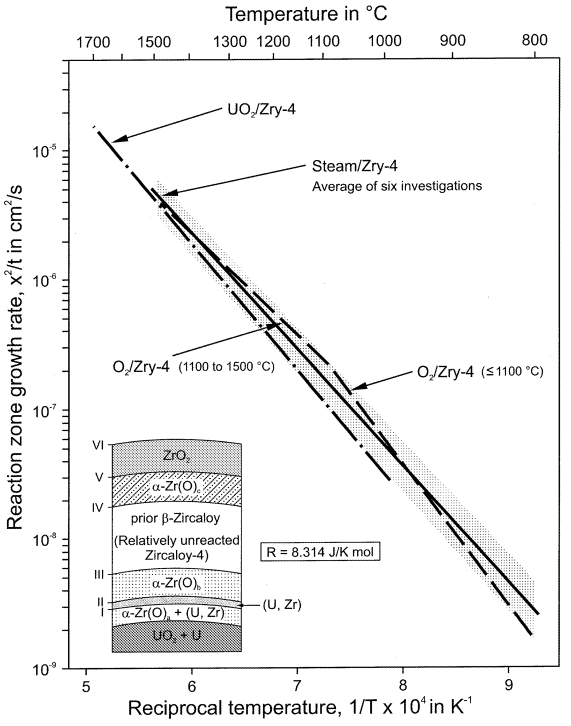

Fig. 3. Reaction zone growth rates for Zircaloy cladding oxidation reactions by UO_2 fuel, steam and oxygen.

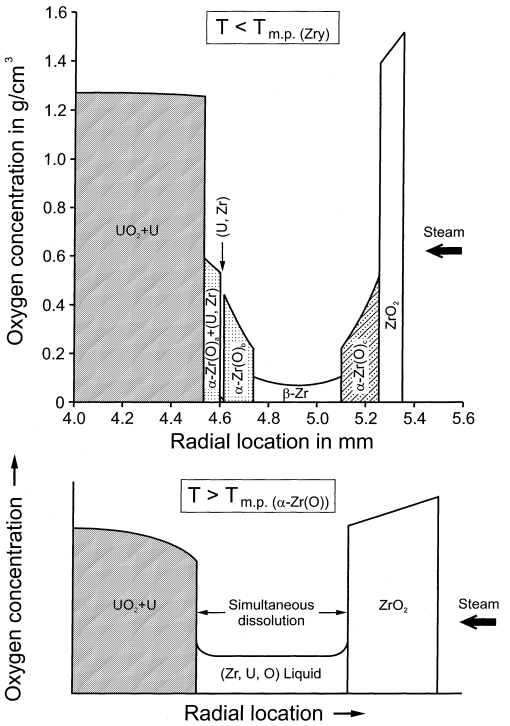

Fig. 4. Formation of various reaction layers and oxygen distribution for simultaneous interactions of solid or liquid Zircaloy with UO_2 and steam.

point of Zircaloy or α-Zr(O) has been reached. Therefore, the relocation of molten material is prevented as long as the ZrO_2 layer remains intact. The molten Zircaloy cladding then interacts simultaneously with UO_2 and the ZrO_2 shell. Fig. 4 shows the conditions for temperatures below and above the melting point of Zircaloy (≈1760°C).

UO_2 and ZrO_2 are dissolved chemically by the molten metallic Zircaloy cladding material; i.e., they are liquefied. This may result in a failure of the ZrO_2 shell and the Zr–U–O melt will be released and causes relocation of UO_2 and ZrO_2 well below their melting points (by about 1000 K). In the cooler lower part of the reactor core, the solidified melts can give rise to cooling channel blockages of different sizes. The relocation of molten cladding terminates its interactions with the fuel and steam.

While UO_2 is dissolved by liquid Zircaloy, a Zr–U–O melt is formed that decomposes into two metallic phases (α-Zr(O) +(U–Zr) alloy) and one ceramic phase ((U, Zr)O_2) during cooldown. When ZrO_2 is dissolved, the Zr–O melt formed decomposes into a metallic (α-Zr(O)) and a ceramic phase (ZrO_2). The ceramic phases are formed only above a critical oxygen concentration in the melts and depend on the amount of dissolved UO_2 and/or ZrO_2.

The kinetics of chemical UO_2 and ZrO_2 dissolution by molten Zircaloy follow parabolic rate laws. In general, the dissolution of solid fuel by molten Zircaloy is very fast; at 2250°C, after 5 min the solidified Zr–U–O melt consists of ≈80 wt% of dissolved UO_2 (Fig. 5; initial molten Zircaloy weight of 9.77 g, melt/solid UO_2 contact area of 5.8 cm [14]). The amount of UO_2 that can be dissolved depends on the quantity, initial oxygen content, and temperature of the Zircaloy melt [14]. Fig. 6 shows an Arrhenius plot of UO_2 dissolution rates and ceramic phase portions in initially oxygen-free molten Zircaloy-4 after the saturation period [14].

Under oxidizing reactor conditions, the Zircaloy also picks up oxygen from the steam. The chemical interaction between Zircaloy and UO_2 will therefore not be as extensive as in an inert environment. As the initial oxygen content of the metallic Zircaloy melt increases, the amount of UO_2 that can be dissolved by the melt decreases; this was experimentally demonstrated in Refs. [15,16].

Despite joint efforts of experimentalists and theoreticians, no common point of view on the physics of the complicated dissolution phenomenon has been developed. The UO_2 and ZrO_2 dissolution kinetics by molten Zircaloy are therefore still under investigation [17,18]. What are needed additionally are experimental data on

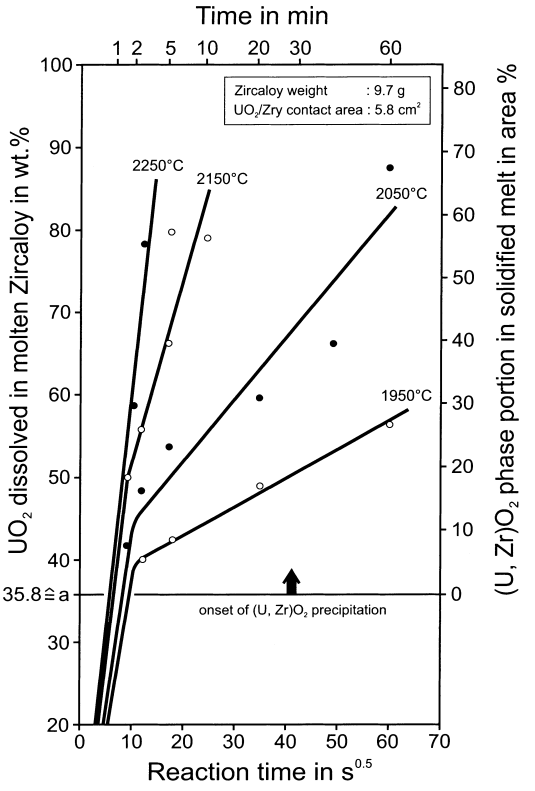

Fig. 5. UO_2/molten Zircaloy dissolution, ceramic phase portions in solidified (Zr, U, O) melts and UO_2 content in molten Zircaloy at different reaction temperatures.

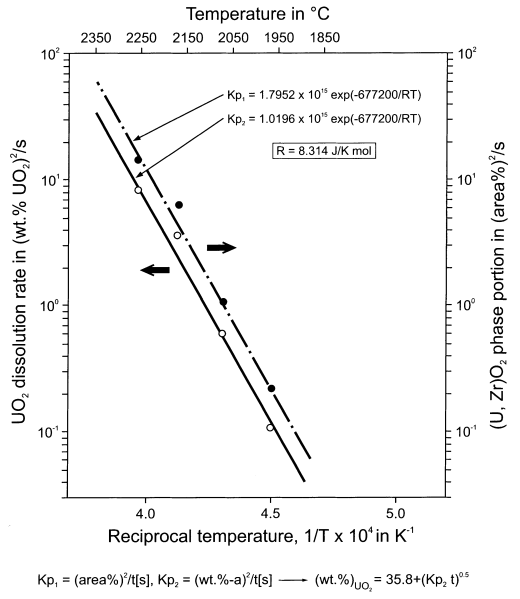

Fig. 6. UO_2 dissolution rates and ceramic phase portions in molten Zircaloy after the saturation period.

the simultaneous dissolution of UO_2 and ZrO_2 by molten Zircaloy.

4.3. U–Zr–O high-temperature phase relations

To understand and to describe the various phase relations in the complex systems Zircaloy/UO_2 and Zircaloy/H_2O, extensive investigations of the phase stability relations in the ternary U–Zr–O-system have been performed up to about 2000°C [4]. The most important features of this ternary system are the existence of an extended central three-phase region (UO_2 + α-Zr(O) + U–Zr melt) as shown in Fig. 7. UO_2 fuel is stable with oxygen-saturated α-Zr(O) (Fig. 8), but not with β-Zr or β-Zr(O) [11]. With regard to the UO_2–Zr interaction, this result explains the observed chemical interaction by which UO_2 is partially reduced to uranium metal as long as zirconium is not saturated with oxygen. The complex reaction layer sequence which forms under solid state conditions is shown in Figs. 2 and 4 and it is explained in detail in Ref. [11]. Since at temperatures >1525°C cubic ZrO_{2-x} coexists with α-Zr(O), a complete range of miscibility between UO_{2-x} and ZrO_{2-x} exists (Fig. 9), resulting in a large two-phase field ((U, Zr)O_{2-x} + α-Zr(O)) instead of a three-phase field (UO_{2-x} + ZrO_{2-x} + α-Zr(O)) that exists below 1525°C (Fig. 7) [4].

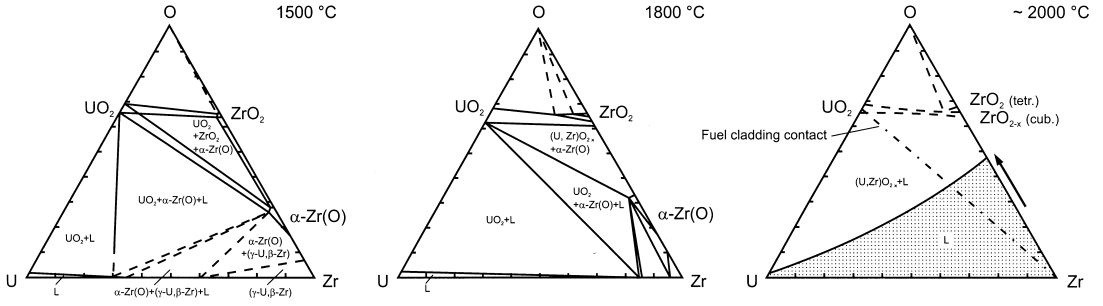

Fig. 7. Equilibrium phase diagrams of the ternary Zr–U–O system at 1500°C, 1800°C and about 2000°C [4].

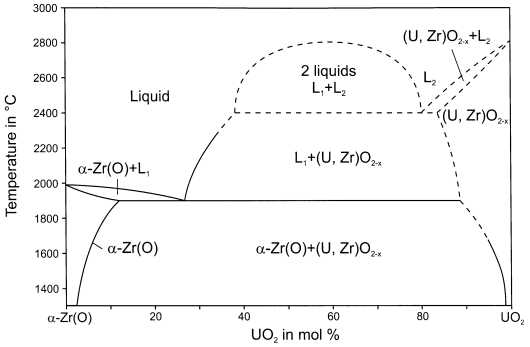

Fig. 8. Phase diagram of the quasi-binary system oxygen-stabilized α-Zr(O) and UO_2 [4].

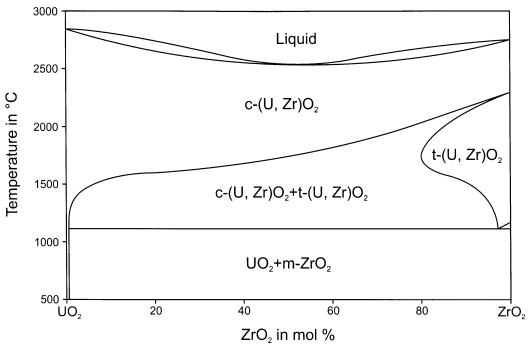

Fig. 9. Phase diagram of the quasi-binary system UO_2 and ZrO_2 [4].

The measured eutectic temperature of the quasi binary α-Zr(O)–UO_2 system is in accordance with the α-Zr(O)–ZrO_2 eutectic temperature of the binary Zr–O system. Very often, the phase relation in the α-Zr(O)–UO_2 system is used and interpreted incorrectly. It can only be used when oxygen-saturated α-Zr(O) is in contact with UO_2. Small deviations in the oxygen concentration of the zirconium result in different phase formations and stabilities [4]. This is especially true with respect to the eutectic temperature and the eutectic point. The eutectic point in the quasi-binary α-Zr(O)–UO_2 system lies at ≈27 mol% UO_2, Fig. 8. The maximum amount of UO_2 that can be completely dissolved at ≈2000°C is ≈28 mol% UO_2, forming a homogeneous Zr–O–U melt. However, about 85 mol% UO_2 can be dissolved at ≈2000°C under the formation of a heterogeneous melt consisting of a U–Zr–O liquid and solid (U, Zr)O_{2-x} particles.

4.4. Chemical interactions between the (Ag, In, Cd) absorber rod alloy and Zircaloy

The absorber rod alloy (80 wt% silver, 15% indium, 5% cadmium) is thermodynamically stable with its stainless steel cladding, even in the liquid state (>800°C). However, the absorber rod guide tube is made from Zircaloy, which will chemically interact with the stainless steel cladding of the absorber rod. During a severe reactor accident, localized contact between stainless steel and Zircaloy exists at many places. This solid-state contact results in chemical interactions with the formation of liquid phases around 1150°C. After failure of the absorber rod cladding, the molten Ag–In–Cd alloy (melting point ≈800°C) comes into contact with the Zircaloy guide tube and chemically destroys it. Then, the molten Ag–In–Cd can even attack and chemically dissolve the Zircaloy cladding of the fuel rods well below the melting point of Zircaloy (≈1760°C). The relocating Ag–In–Cd alloy is therefore able to propagate and accelerate the core-melt progression at rather low temperatures.

The chemical interactions between Ag–In–Cd and Zircaloy were studied in separate-effects tests which are described in Ref. [19]. The reaction zone growth rate (decrease in Zircaloy wall thickness) is plotted in an Arrhenius diagram against the reciprocal temperature in Fig. 10. At temperatures >1200°C, the chemical interactions result in a sudden and complete liquefaction of the compatibility specimens. As a consequence, the

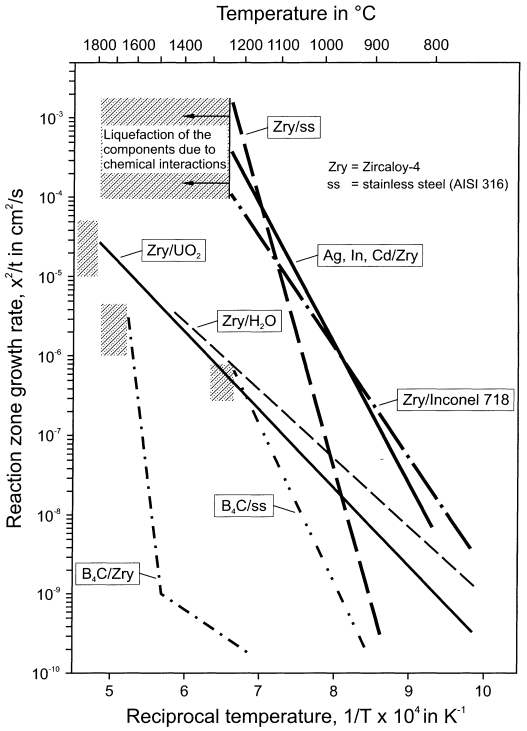

Fig. 10. Total reaction zone growth rates of various reaction couples of fuel element components. In most cases liquefaction of the materials occurs below their melting points.

Zircaloy cladding can be chemically dissolved ≈600 K below its melting point and may even result in a low-temperature UO_2 fuel dissolution. For phase considerations of melting reactions, the quaternary U–Zr–Fe–O system may be regarded as a model system for the complicated multi-component system of a beginning core melt; iron represents the stainless steel. A detailed description of the phase relations is given in Ref. [4].

The chemical interaction between the Ag–In–Cd alloy and Zircaloy is theoretically described by a model under conditions of convective mixing in the (Zr, Ag, In) liquid phase in Ref. [20]. Homogeneous bulk saturation of the liquid phase with Zr takes place in the course of the Zircaloy dissolution by the absorber melt resulting in a gradual decrease of the interaction process. Two main parameters of the model are calculated: Zr concentration in the saturated melt and convective mass transfer coefficient in the liquid phase [20].

4.5. Chemical interactions between Zircaloy and stainless steel or Inconel

The Zircaloy/stainless steel (1.4919; corresponds to ss Type 316 with 18 wt% Ni and 8 wt% Cr) interactions are important with respect to the contact between the absorber rod cladding and the Zircaloy guide tube and between the Inconel spacer grid and the Zircaloy fuel rod cladding. In both cases, the iron–zirconium and the nickel–zirconium phase diagrams show that due to eutectic interactions, early melt formation has to be expected, which initiates the melt progression within the fuel assembly at low temperatures. Liquid phases form at temperatures <1000°C; however, the reaction kinetics become significant only above 1100°C. This was seen in the CORA tests, where fuel rod bundles were heated up to complete meltdown. In all cases, the damage of the bundle was initiated due to Zircaloy/stainless steel and Zircaloy/Inconel interactions. Localized liquefaction of these components started around 1200°C [6].

The reaction kinetics between Zircaloy and stainless steel can be divided into a reaction zone growth rate in Zircaloy and one in stainless steel, as shown in Fig. 11. One can see that the Zircaloy is attacked more strongly than the stainless steel. Oxide layers on the Zircaloy cladding outside diameter delay the chemical interactions between Zircaloy and steel, but they cannot prevent them. The influence of oxide layers becomes less important at temperatures >1100°C, since the dissolution of the protecting ZrO_2 layers occurs rather fast and the stainless steel is then in contact with metallic Zircaloy or oxygen-stabilized α-Zr(O) [21].

In a first approach, the reaction behavior of Zircaloy with Inconel 718 is comparable to that with Type 316 stainless steel [22]. At temperatures <1100°C, Inconel attacks the Zircaloy faster than stainless steel; above 1100°C, the situation is the reverse. In both cases, the melting of a relatively large quantity of Zircaloy with limited melting of the adjacent stainless steel or Inconel takes place. During heat-up of the stainless steel/Zircaloy and Inconel/Zircaloy reaction systems, a sudden and complete liquefaction of the specimens occurs at temperatures slightly above 1250°C. This may be the reason that melt progression in a fuel rod bundle initiates at absorber rod cladding (stainless steel)/Zircaloy guide tube contact areas and Inconel spacer grid/Zircaloy fuel rod contact locations [6].

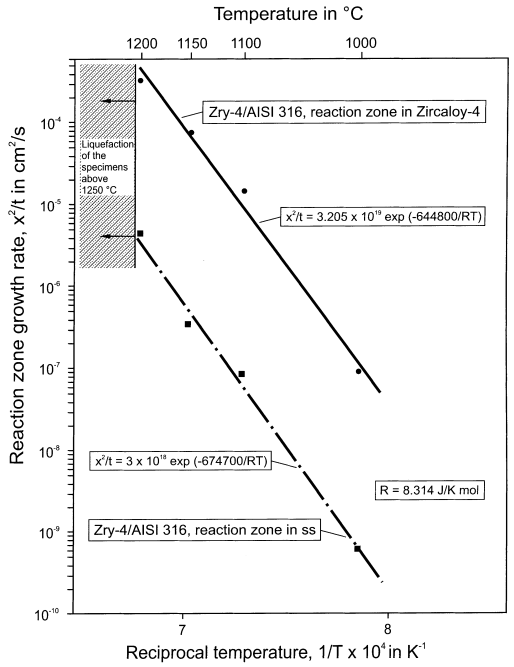

Fig. 11. Reaction zone growth rates in the reaction couple Zircaloy/stainless steel; comparison of the reaction zone growth rates in Zircaloy and stainless steel (AISI 316).

4.6. Reaction behavior of B_4C absorber material with stainless steel or Zircaloy

The absorber rods in boiling water reactors (BWRs), Russian VVER-1000 type reactors and some pressure water reactors (PWR) consist of boron carbide (B_4C) pellets or powder in stainless steel tubes. In BWRs, the absorber rods are contained in a four-blade stainless steel assembly. Four fuel rod bundles are each surrounded by a Zircaloy channel box arranged around the cross-shaped control element. The B_4C/stainless steel system is not thermodynamically stable; i.e., chemical interactions are expected at temperatures above 800°C. After failure of the absorber rods the B_4C may then also interact with the Zircaloy flow channel box and the adjacent UO_2/Zircaloy fuel rods. For this reason, the

chemical interactions between B_4C and Zircaloy have also to be known.

The reaction kinetics for the B_4C/stainless steel and B_4C/Zircaloy systems can be described by parabolic rate laws [23]. The experimental results show that the complete failure of the B_4C/Zircaloy reaction couple as a result of liquefaction occurs at ≈1650°C, which is 400 K higher than that of the B_4C/stainless steel reaction system at ≈1250°C (Fig. 10). In both reaction systems, the liquefaction occurs below the melting points of the components due to eutectic interactions. If Zircaloy is used for the cruciform absorber element instead of stainless steel, the onset of liquid phase formation could be shifted to much higher temperatures. Besides, at temperatures <1200°C, the B_4C/Zircaloy reaction rate is much lower than that of B_4C/stainless steel. Therefore, more time would be available during a severe accident for accident management measures.

The chemical interaction kinetics between B_4C and stainless steel and Zircaloy have been described by analytical models [24,25]. The proposed models can be applied not only for modeling of isothermal tests (on which basis they are developed), but also for more complicated non-stationary transient temperature conditions which are typical for integral experiments like the CORA fuel bundle meltdown tests [6] as well as for anticipated real severe accident conditions in nuclear power plants.

The premature low-temperature failure of the BWR absorber element and its relocation may result in an early localized relocation of the B_4C absorber material within the reactor core and may cause local criticality problems in a severe reactor accident if the core is flooded by unborated water. In the CORA 16 experiment, in which a BWR fuel rod bundle was heated out-of-pile up to 2000°C, the failure of the absorber element and its relocation between 1200°C and 1300°C was confirmed long before the fuel rods failed.

5. Integral experiments on fuel element behavior

In the previous sections the high-temperature material behavior of various material combinations is described. However, what is of interest is the integral behavior of the different fuel element materials with increasing temperatures under realistic boundary conditions. Therefore, in the framework of the CORA Program out-of-pile integral experiments with 2 m long PWR, BWR and VVER-1000 fuel rod bundle simulators (with 1 m heated length), containing a maximum of 57 rods, were performed [6]. Altogether 19 bundle experiments were performed under flowing steam up to about 2400°C. Of particular importance has been the determination of critical temperatures, above which liquid phases form as a result of chemical interactions between the fuel element components or by reaching a melting point and their influence on damage propagation. On the basis of the experimental results and thermodynamic consideration, three distinct temperature regimes can be defined where liquid phases that form in the reactor give rise to substantial material relocations and different degrees of core damage [6].

5.1. Temperature regimes for liquid-phase formation

5.1.1. Temperature regime between 1200°C and 1400°C

At temperatures between 1200°C and 1400°C (Fig. 12), the Ag–In–Cd control rods may possibly start to fail directly as a result of chemical interactions between the stainless steel cladding of the absorber rods and the Zircaloy guide tube or by simple mechanical rupture of the cladding (low system pressure case). However, in some situations, failure could be delayed until stainless steel melts at ≈1400°C (high system pressure case). The failed absorber rod releases the liquid Ag–In–Cd alloy, which melts at ≈800°C. This alloy interacts eutectically with Zircaloy, but not with stainless steel, and can liquefy the Zircaloy much below its melting point (≈1760°C). This enables the damage to propagate to neighboring Zircaloy-clad fuel pins. The associated liquefaction and relocation can open axial and radial flow pathways through the whole core. Since

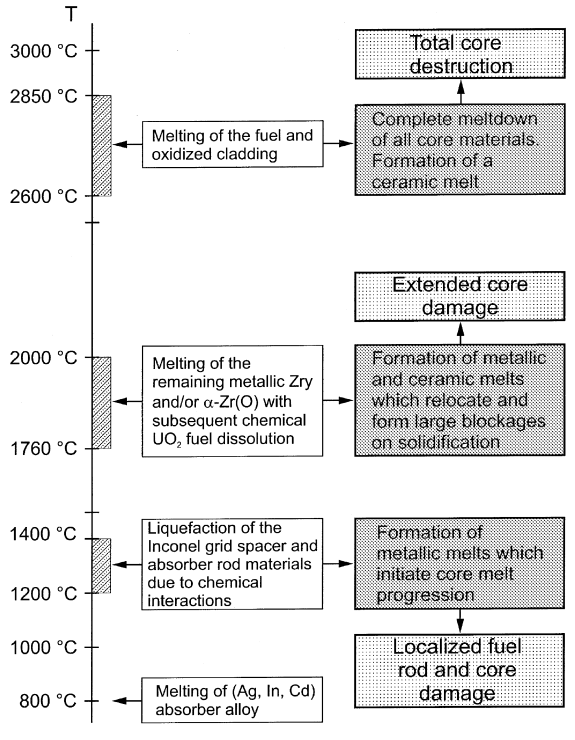

Fig. 12. Temperature regimes for extended liquid phase formation in a severe reactor accident.

the solidification temperatures of these material mixtures are extremely low, they should reach the lower core structures first, or they may fall into the water below the core, and ultimately into the lower head of the RPV, and cause additional steam generation, which may temporarily overcome steam starvation in some of the upper portions of the core. Due to the low-temperature failure of the control rods and fast relocation to colder parts of the core, cadmium vaporization is reduced.

Boron carbide (B_4C), which is used as absorber material in BWRs, VVERs and some PWRs may also be liquefied above 1200°C, due to eutectic interactions with the stainless steel cladding tubes. The B_4C control rod material separates from fuel rod materials by relocation processes in the liquid state. Therefore, reflood water must be sufficiently borated to avoid recriticality and power generation during early phase core degradation, which means prior to the disintegration of the core into a rubble bed.

Other low-temperature eutectic interactions can occur between the Zircaloy of the guide tube and the Inconel of the spacer grids. At ≈1250°C, these interactions result in a localized failure of the fuel rods, the formation of molten phases, and the relocation of liquefied Zircaloy cladding material far below its melting point. This type of fuel rod failure mode causes early fission product release in a high-pressure accident scenario. In a low-pressure scenario, the cladding will balloon and rupture even at much lower temperatures, with release of the gap fission product inventory.

5.1.2. Temperature regime between 1800°C and 2000°C

Between 1800°C and 2000°C, the unoxidized portions of the Zircaloy cladding of the fuel rods, which are still metallic, start to melt and can chemically dissolve the solid UO_2 fuel and the ZrO_2 surface layer that oxidation is producing on the cladding outside diameter. The amount of unoxidized cladding depends on the heat-up rate and steam availability. The molten metallic Zircaloy then relocates downward along the individual rods in a slow 'candling' process or by a fast 'dropping' process and is so removed from the higher temperature regions of the core where quicker oxidation prevails. These processes can notably limit the uncontrolled temperature escalation and the corresponding rapid hydrogen generation caused by Zircaloy oxidation.

Molten metallic Zircaloy can chemically dissolve large quantities of solid UO_2 fuel and 'liquefy' it at ≈1800°C, that is ≈1000 K below the melting point of UO_2 (≈2850°C). Due to this liquefaction process, starting at ≈1800°C, low-temperature melt relocations of Zr–U–O mixtures containing decay heat sources takes place. This relocation is also part of the so-called candling process. Solidification and melting occur repeatedly as water boils off and core melt progression proceeds. At the same time, molten metallic Zircaloy can also chemically dissolve ZrO_2 and breach the ZrO_2 shell on the cladding surface.

5.1.3. Temperature regime between 2600°C and 2850°C

In regions of the core where temperatures between 2600°C and 2850°C may be reached, the (U, Zr)O_2 solid solution, which may form in the fuel pin during a slow core heat-up or as a result of UO_2 dissolution by molten Zircaloy, starts to melt and relocate. At temperatures >2850°C, all components of the reactor core and chemically formed phases are molten, including UO_2 itself, which has the highest melting point (≈2850°C). The melting point of ZrO_2 is about 2700°C.

The different temperature regimes result in different core damages (Fig. 12). Regime 1 causes localized core damage and the blockages formed will be probably coolable. In temperature regime 2, much stronger melt formation occurs with extended core damage and the generation of core regions that can no longer be cooled. Regime 3 finally results in the complete meltdown of all materials and a total destruction of these high-temperature core regions.

Evidence for all these molten phases and relocation processes has been seen in the various in-pile (ACRR, PBF, LOFT, NRW FLHT, PHEBUS) and out-of-pile (CORA) experiments and in TMI-2 [5–10]. The various molten phases solidify on cool-down at different temperatures and may therefore form blockages at different axial locations, although the undestroyed spacer grids may define the limit of axial slumping. It is not yet clarified to what extent the flow channel blockages affect the boil-off steam flow rate, and as a consequence, the Zircaloy oxidation and hydrogen generation, although the disruption of core geometry and flow paths caused by the core slumping probably would decrease Zircaloy oxidation efficiency within the core.

5.2. Influence of heat-up rates on liquefaction of materials

In addition to the temperature of the core, the local heat-up rates also have an important influence on the in-vessel core melt progression. These local heat-up rates can be largely controlled by local steam availability because of the importance of the exothermic Zircaloy/steam reaction. At initial low heat-up rates <0.5 K/s, the fuel cladding is completely oxidized to ZrO_2 under steam-rich conditions before reaching the melting point of metallic Zircaloy. As a result, fuel rod melting will not occur until 2600°C. At initial heat-up rates above 1 K/s, temperatures are reached that permit the Zircaloy metal to melt and dissolve UO_2 before all the Zircaloy becomes oxidized. The melt may not relocate because it can be held in place by the solid ZrO_2 layer that is formed during heat-up on the surface of the Zircaloy cladding. Zircaloy oxidation may also be limited by

steam starvation. At high heat-up rates >5 K/s, the ZrO_2 layer will probably be too thin to hold the metallic melt in place and relocation will occur after mechanical and/or chemical breach of the ZrO_2 shell (Fig. 13).

It is evident from the foregoing discussion that the in-vessel melt progression process is very complex. It can only be understood by a combination of experiments and computer modeling and careful verification and validation of such codes. This requires detailed and thorough analysis of the out-of-pile and in-pile tests, the large-sized LOFT LP-FP2 experiment, and the TMI-2 accident. Both TMI-2 and LOFT LP-FP2 can be linked to smaller scale separate-effects tests to look at particular phenomena. The computer models, when validated against these smaller scale experiments, must allow application to reactor plant conditions where scaling effects become important.

5.3. Material distribution in integral experiments

The materials redistribution within the various types of fuel elements examined in the integral test program

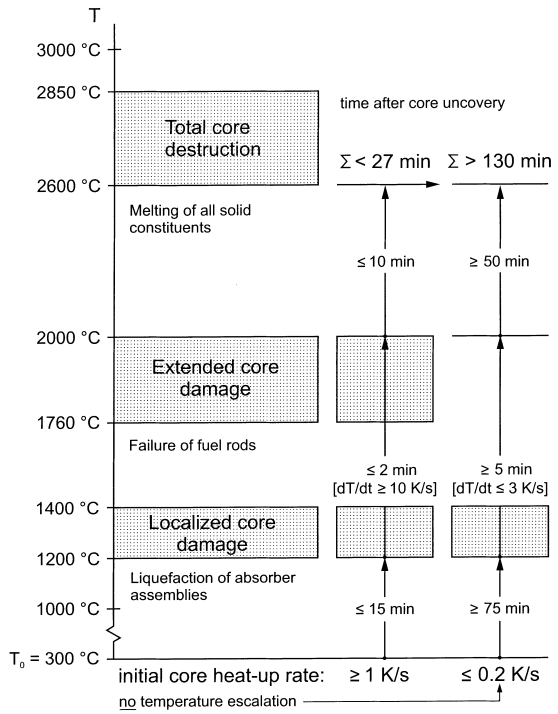

Fig. 13. Dependence of the temperature regimes on liquid phase formation on the initial heat-up rate of the core. Small heat-up rates drastically reduce the amount of molten Zircaloy (1800–2000°C) and give more time for possible accident management measures.

CORA showed interesting results [26]. The absorber materials initiate melt formation and melt relocation and shift the temperature escalation as a result of the zirconium–steam reaction to the lower end of the bundle by the relocation, i.e., by movement of molten (hot) material. The relocation of melts occurs by rivulet and droplet flow. The various melts solidify on cool-down at different temperatures, i.e., at different axial locations. The viscosity of the molten material has an impact on the relocation behavior and has to be considered in modeling of these phenomena [37]. Material relocations induce a temperature escalation at about 1200°C. The release of chemical energy results in renewed melt formation and relocation. Therefore, the processes are closely coupled. Pre-oxidation of the cladding results in reduced melt formation and shifts the onset of temperature escalation to higher temperatures. Inconel and stainless steel spacers relocate above 1250°C as a result of chemical interactions and do not act as materials catchers. Pre-oxidized Zircaloy spacers still exist at temperatures >1700°C and therefore have a significant impact on the relocation processes at lower temperatures [26].

The CORA-10 test simulated the behavior of a rod bundle with additional cooling at its lower end (TMI-2 conditions) [34]. Fig. 14 depicts the axial bundle temperature profile at different times and the material relocation. One can recognize the influence of the higher heat losses at the lower end (30 cm) of the bundle in the axial temperature profiles. Two steep axial temperature gradients form at 4400 s, one at 45 cm and one at the 30 cm bundle elevation. Corresponding to the steep axial temperature gradients, the main blockage formed at the 40 cm bundle elevation. The absorber rods cannot be found in the cross sections as a result of liquefaction and relocation. A part of the UO_2 was dissolved by molten Zircaloy and relocated [26].

The axial material distributions of CORA-W1 [35] and CORA-W2 [36] are compared in Fig. 15, together with the boundary conditions of the experiments. The two tests were performed with fuel-element components typical of Russian type VVER-1000 reactors, Zr 1% Nb fuel rod cladding, and B_4C absorber material in stainless steel cladding. Fig. 15 underlines the extraordinary influence of the low-temperature eutectic interaction between B_4C and stainless steel on melt relocation, damage progression, and blockage formation. The absorber material interactions initiate the formation of liquid phases. Relocating melts transport heat to lower bundle positions and initiate the exothermic zirconium–steam reaction, which leads to a renewed temperature increase, melt formation, and relocation. Compared with the CORA-W1 bundle, the axial region of fuel rod damage in the CORA-W2 bundle extended to the very lowest end of the bundle, despite the fact that the input of electrical energy was smaller [26].

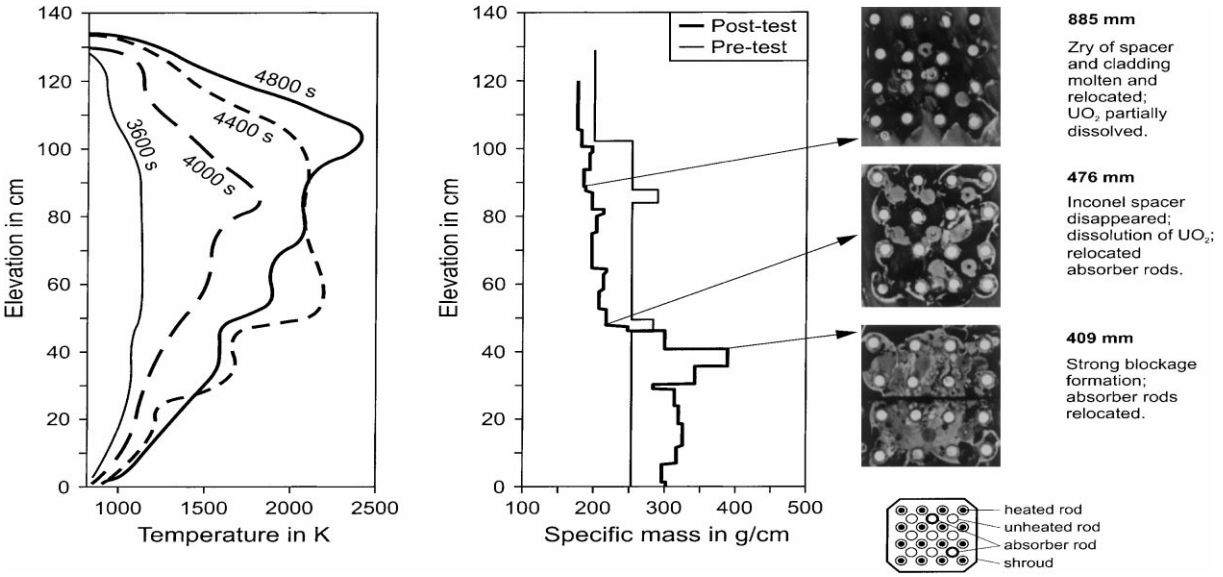

Fig. 14. Axial bundle temperature profile and material relocation in the bundle melt down experiment CORA-10; simulating TMI-2 accident conditions with cold lower end [26].

6. Molten material relocation into the lower plenum

As emphasized in the TMI-2 accident, the transfer mode of molten material from the degraded core to the lower head of the vessel is an important factor in the evaluation of the in-vessel progression of a severe accident in nuclear reactors. The understanding of this phenomenon is very important with respect to the in-vessel debris cooling and vessel failure analyses.

Early phase (metallic phase melting) and late phase (ceramic phase melting) core damage progression affect the initial conditions for material relocation. Metallic blockage formation in the lower core region, melt pool growth and crust failure behavior are important factors in determining the quantities, rate and mode of melt/material transfer to the lower head. Melt relocation processes into the lower plenum may also depend on the differences in core damage conditions relevant to the type of nuclear reactor under examination. Generally, the TMI-like 'wet-core' scenario, typical for PWRs, contrasts with a BWR-typical 'dry-core' scenario. As demonstrated by the TMI-2 accident, the 'wet-core' conditions enhance large molten pool formation with coherent molten mass relocation after crust failure; while gradual melt relocation is more likely under 'dry-core' conditions.

Depending on the considered scenario, molten material relocation into the lower plenum may occur from the lateral periphery of the core or from the core bottom. In both cases, the thermal–mechanical attack of the melt on the surrounding metallic support structures (lower core plate, core baffle, barrel, etc.) should be taken into account. The degradation of these structures by ablation and melting may produce an enlarged pathway towards the lower head that may affect the rate of melt relocation.

Significant amounts of molten material relocated to the lower head could directly threaten the vessel integrity by steam explosion due to melt interaction with the water still present in the vessel, or by jet impingement on the lower vessel wall. Metals such as Zircaloy in the melt may enhance the energy release in case of a steam explosion and the interaction of the melt jet on the vessel wall.

The threshold of failure of the reactor-vessel lower head determines whether or not the reactor vessel fails for given melt conditions and vessel pressure. Such failure is of major significance. The threshold and the mode of failure under melt attack determine the mass and the rate of release of the melt into the containment. Such a melt attack on the internally-flooded vessel lower head did occur in the TMI-2 accident, but the lower head did not fail.

The consequences of reflooding a severely degraded core at different stages of core degradation are also of LWR safety significance. Of primary concern is whether or not, at a given state of core damage, reflooding will promptly terminate the accident, as it did not do at TMI-2. The large amount of generated hydrogen (with local core heating) from Zircaloy oxidation by the reflood steam, the amount of reflood steam, and the possibility of a large steam explosion are also of reactor safety interest.

Most of our knowledge in severe fuel damage and core-melt progression is based on observation from

fresh-fuel experiments. However, the small number of experiments with irradiated fuel may exhibit lower temperature thresholds for slumping and melting, and may under certain conditions foam and swell.

The PHEBUS program currently underway in France [10] will provide additional experimental evidence in the area of irradiated fuel effects (the FPT1 test has evidenced differences between the degradation of fresh and irradiated fuel rods). Melt progression behavior under conditions of air ingression, as would be associated with a shutdown accident during refueling, is another little studied area where uncertainties remain. The fact that the only data available on the physical process of core material release and transfer to the lower plenum are from the TMI-2 accident, limits the ability to assess thoroughly models describing these processes.

While there is a significant number of experiments which address the early (mainly) and late phase core degradation (PBF-SFD [5], ACRR DF and ST [7], CORA [6], LOFT LP-FP-2 [5,7], PHEBUS-SFD [9]), which allow development and validation of code modeling, no significant experimental work has been done (except the Sandia XR tests [7]) to investigate molten material relocation processes to the lower head. The present knowledge is mainly based on the analysis of the TMI-2 accident [8]. Therefore severe accident codes, both mechanistic (e.g., SCDAP/RELAP5, ICARE/CATHARE, ATHLET-CD/KESS) and integrated (e.g., MELCOR, MAAP4, ESCADRE), are more or less able to calculate the initial conditions for melt relocation (temperature, composition and amount of melt), but rely on empirical and simplified (user specified) models for the evaluation of material relocation into the lower plenum.

In an OECD/NEA status report [27] the current state of knowledge of molten material relocation into the lower plenum, the main severe accident scenarios envisaged for both PWRs and BWRs, and boundary conditions are summarized. Consequences of movement of material to the lower head are considered with respect to the potential for reactor pressure vessel failure. The models available in the above-mentioned computer codes dealing with molten material relocation into the lower plenum are described.

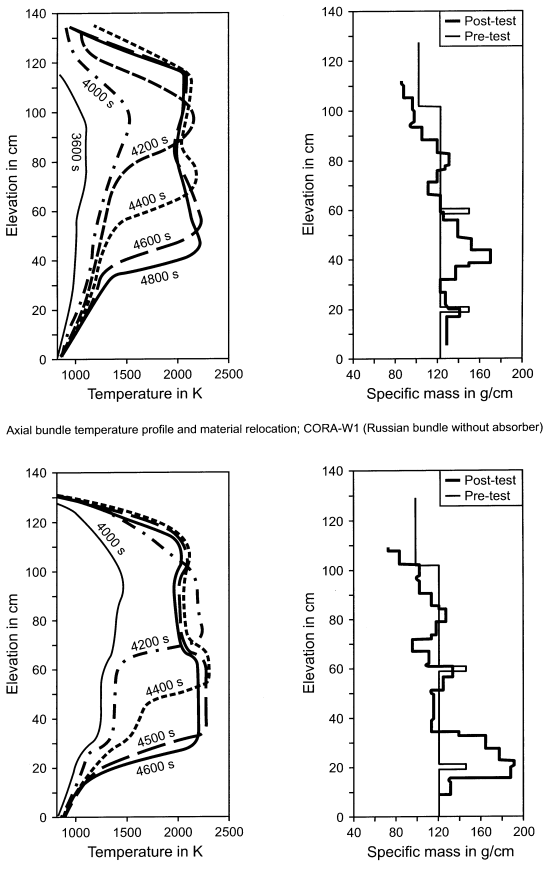

Fig. 15. Influence of the B_4C/stainless steel absorber rod liquefaction on bundle degradation and material distribution in the VVER tests CORA-W1 and CORA-W2; the melt progression and relocation behavior of the B_4C absorber rod is comparable to that in BWRs [26].

7. Investigation on hydrogen generation during flooding

One of the still open problems on early phase core degradation is the hydrogen generation during quenching [6,28,31]. The most important accident management measure to terminate a severe accident transient in a LWR is the injection of water to cool the uncovered degraded core. Analysis of the TMI-2 accident and the results of integral out-of-pile (CORA) and in-pile experiments (LOFT, PHEBUS, PBF) have shown that before the water succeeds in cooling the fuel pins there will be an enhanced oxidation of the Zircaloy cladding that in turn causes a sharp increase in temperature, hydrogen production and fission product release. Quenching is considered a worst case accident scenario regarding hydrogen release rates to the containment. The increased hydrogen production worries those concerned with reactor safety. For in- and ex-vessel hydrogen management measures, one has to prove that the hydrogen release rates and total amounts do not exceed safety-critical values for the considered power plant. In most of the code systems, describing severe fuel damage, the quench phenomena are either not considered or only modeled in a simplified empirical manner.

Although nobody suggests not quenching the core, it is important that the hydrogen generation rate is known so that accident mitigation measures can be designed appropriately:

- Passive autocatalytic recombiners work slowly and their surface area has to be sized.
- The concentration of hydrogen in the containment may be combustible for only a short time before detonation limits are reached. This limits the period during which igniters can be used.

No models are yet available to predict correctly the quenching processes in the CORA and LOFT LP-FP-2 [31] tests. No experiments have been conducted that are suitable for calibrating the models. Since the increased hydrogen production during quenching cannot be determined on the basis of the available Zircaloy/steam oxidation correlations, new experiments are therefore necessary. An extensive experimental database is needed as a basis for model development and improvement [28,29].

In the earlier CORA program only a small number of quench tests could be performed [6,30]. These experiments showed that quenching of the hot bundles by water resulted in a renewed temperature escalation at the top of the bundle and additional hydrogen generation, although the electric power supply was shut off.

The comparison of the quantitative data on hydrogen production measured between the CORA-16 BWR-related test (without quenching) and CORA-17 (with quenching) in Fig. 16 shows a remarkable hydrogen peak during the flooding phase of CORA-17. Similar

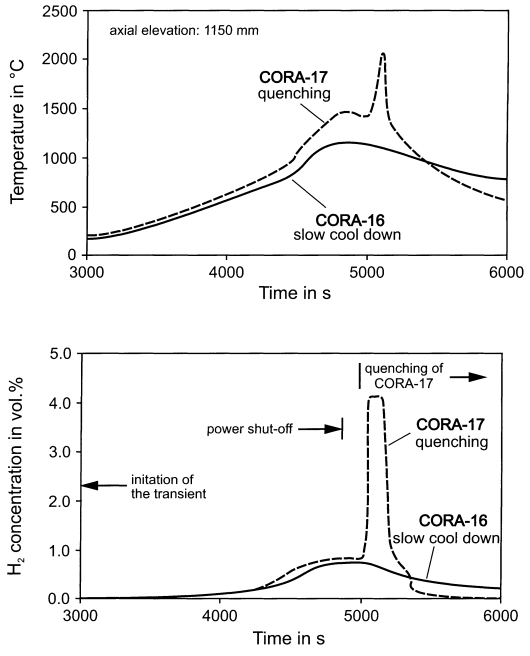

Fig. 16. Hydrogen generation measured during the CORA-16 and CORA-17 BWR-type tests without and with quenching, respectively. Quenching (flooding) of the hot bundle results in a temperature increase and remarkable hydrogen peak.

behavior in the hydrogen response was observed in PWR-related tests, although it is assumed that in the BWR tests, additional energy and hydrogen production was caused by a steam reaction with the remnant B_4C absorber (B_4C oxidation in steam is more exothermic and produces more hydrogen per gram material than does Zircaloy) [6,30].

The Forschungszentrum Karlsruhe has started a QUENCH program on the determination of the hydrogen source term to investigate the generation of new metallic surfaces by cracking and fragmentation of the oxygen-embrittled cladding tubes as a result of the thermal shock during flooding and their influence on enhanced oxidation and hydrogen generation [38,39].

A small scale test rig was built in which it is possible to quench short Zircaloy fuel rod segments by water (90°C and 1.5 cm/s flooding rate) or to rapidly cool the rods by injected steam (140°C and 2 g/s). The main experimental parameters investigated are: the extent of cladding pre-oxidation (0, 100, 300 μm ZrO_2 layer thickness) and the temperature of the Zircaloy tube at onset of quenching (1200°C, 1400°C and 1600°C) [29]. The heat losses in these experiments were such that no temperature escalation was seen. The mechanical behavior of the cladding tube depends on the initial oxide scale thickness and the tube temperature at onset of quench. Large cracks, penetrating the oxide layer and α-Zr(O) metal substrate, can be observed in water-quenched and steam-cooled specimens with an initially 300 μm thick oxide layer thickness. The formation of the crack is more pronounced if the quench is initiated from low temperatures (1200°C). The surfaces of the cracks are partially oxidized. This indicates that the cracks are already formed at high temperatures and that they therefore contribute to the hydrogen generation [29].

Some of the typical thermohydraulic boundary conditions during quenching of a reactor core can only be simulated by large-scale bundle tests. An experimental facility (QUENCH), which allows the quenching of bundle simulators under nearly adiabatic conditions, was constructed at the Forschungszentrum Karlsruhe, in which a bundle of 21 rods of about 2.5 m total length will be quenched. The main component of the test facility is the test section with the test bundle simulator. The rods are arranged on a PWR-type square pitch within a circular shroud and are heated internally by tungsten resistance heaters over a length of about 1 m. The fuel rod simulators are similar to those employed in the CORA program, with the exception that zirconia rather than uranium dioxide pellets are used. The shroud is composed of Zircaloy which is surrounded by a thick insulating layer of fibrous zirconia surrounded by an argon cooling jacket (Fig. 17). The hydrogen is analyzed by two different instruments: (1) a mass spectrometer located at the off-gas pipe, and (2) A 'CALDOS' hydrogen detection system located behind the

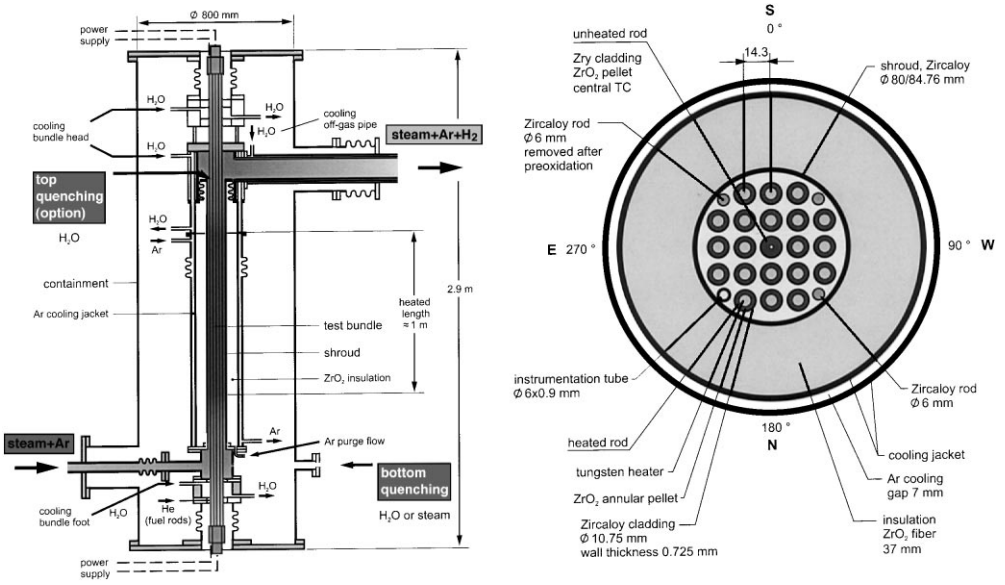

Fig. 17. Schematic of the test section of the new QUENCH Facility and of the fuel rod simulator bundle cross section. Quenching occurs either at the bottom or at the top of the bundle by water or by 'cold steam' injection.

main stream condenser. Commissioning tests have been performed in October 1997 [38]; the first bundle quench experiments QUENCH-01 and QUENCH-02 [39] have been conducted in February and July 1998, respectively.

8. Conclusions; principal remaining uncertainties

The *early-phase of core degradation* has been extensively studied by separate-effects [4,6,32] and integral experiments [5–7,9]. Additional representative tests remain necessary for model development and validation on the following degradation aspects [2,7]:

- Simultaneous dissolution of UO_2 and ZrO_2; failure conditions of the outer ZrO_2 layer on Zircaloy cladding tubes by molten Zircaloy.
- Oxidation of relocating and relocated Zr-rich melts, which affects part of the power distribution during fuel rod degradation and melt relocation.
- Rapid cooling (quenching) of degraded cores, including fuel rod embrittlement, enhanced oxidation and hydrogen generation.
- Impact of fuel degradation on fission product release, particularly in case of fuel dissolution by molten Zircaloy and during quenching of degraded cores.
- Effects of irradiated fuel on fuel failure, fuel dissolution and core degradation.

There exists a large data bank from integral early-phase experiments (temperatures up to 2500°C, with limited core material relocation). These data have been obtained under a large range of conditions and are complementary. They cover different LWR bundle designs, different heating methods and initial heat-up and cooling rates, including rapid cooling representative of final quenching. The high-temperature material behavior of the Russian VVER-1000 bundles was found to be comparable with that observed in the PWR or BWR tests of Western design. The data bank enables good understanding of the different severe fuel damage processes up to the final cooling. However, quench-related materials phenomena, such as cracking of ZrO_2 oxide shells which may lead to renewed heat-up and hydrogen generation, are not well understood and need further study.

Although the data bank on early-phase core degradation is comprehensive, the close coupling amongst the different phenomena means that quantification of individual effects is not always possible. This limits the usefulness of the data for model development [2].

Late-phase of core degradation involves melt behavior at temperatures above about 2500°C, and also the premelting behavior of solid ceramic debris, including fuel swelling and foaming, fuel fragmentation, and fuel slumping. The mass and the other characteristics of the ceramic melt released from the core into the lower plenum water are determined by late-phase melt progression processes, in particular the mechanism and threshold of the melt-through of the ceramic melt pool from the core and also the location of melt-through [7,27].

The behavior of late-phase core materials in defined geometries (e.g. debris bed, melt pool) is fairly well understood. The database on transition processes (e.g. formation of a debris bed from embrittled and cracked

rod stacks, melt pool formation, and relocation of material into the lower head) is much poorer. Here, the PHEBUS FP test program is starting to produce significant extensions to current knowledge [10]. The existing data base, which has come primarily from the TMI-2 post accident core examinations [8], has been broadened by data from tests such as the Sandia-MP and -XR series [7], and from tests on melt pool thermal hydraulics. However, large uncertainties limit the possibilities of extending these results to predict late-phase behavior and vessel rupture in other severe accident conditions. The limited knowledge is reflected in the simplification of models at present incorporated in the severe accident codes [27]. Further investigations should be mainly addressed to the molten chemical–mechanical material interactions (ablation and perforation) with the core support structures, which may influence the pouring rate and the transfer mode of molten material to the lower head of reactor vessel (either coherent or gradual melt relocation).

The late phase is of key importance for plant safety studies in such areas as hydrogen generation (flooding of degraded cores in the late phase), fission product release, initial conditions for melt/coolant interactions, and wall vessel attack [2,7]. Increased emphasis is given to these topics in the European Union 4th Framework Programme [40].

Acknowledgements

I would like to thank Dr T. Haste (AEA Technology, UK) for his thorough review of the paper and valuable remarks.

References

[1] G. Van Goethem, W. Balz, E. Della Loggia, FISA-95, European Union research on severe accidents, European Union Report 16896, 1996.
[2] T. Haste, B. Adroguer, U. Brockmeier, P. Hofmann, K. Müller, M. Pezzilli, In-vessel core degradation in LWR severe accidents, European Union Report 16695, 1996.
[3] T. Haste, B. Adroguer, R.O. Gauntt, J.A. Martinez, L.J. Ott, J. Sugimoto, K. Trambauer, In-vessel core degradation code validation matrix, OCDE/GD (96) 14 (1996).
[4] P. Hofmann, S. Hagen, G. Schanz, A. Skokan, Nucl. Technol. 87 (1989) 146.
[5] R.R. Hobbins, D.A. Petti, D.J. Osetek, D.L. Hagrman, Nucl. Technol. 95 (1991) 287.
[6] P. Hofmann, S. Hagen, V. Noack, G. Schanz, L. Sepold, Nucl. Technol. 118 (1997) 200.
[7] R.W. Wright, Nucl. Sci. Technol. 24 (1996) 283.
[8] Special issue on Materials interactions and temperatures in the TMI-2 core, Nuclear Technology, vol. 87/1, 1989, pp. 13–326.
[9] C. Gonnier, G. Geoffroy, B. Adroguer, PHEBUS SFD programme, main results, in: ANS Proceedings, ANS Meeting, Portland, 1991, p. 76.
[10] P. Von der Hardt, A. Jones, C. Lecomte, A. Tattegrain, Nucl. Safety 35 (1994) 2.
[11] P. Hofmann, D.K. Kerwin-Peck, J. Nucl. Mater. 124 (1984) 80.
[12] D.R. Olander, J. Nucl. Mater. 115 (1983) 271.
[13] P. Hofmann, J.H. Neitzel, E.A. Garcia, Chemical interactions of Zircaloy with UO_2 fuel and oxygen between 900 and 2000°C, Experiments and PECLOX code, Kernforschungszentrum Karlsruhe report no. KfK-4422, 1988.
[14] P. Hofmann, H. Uetsuka, A.N. Wilhelm, E.A. Garcia, Dissolution of solid UO_2 by molten Zircaloy and its modeling, in: International Symposium on Severe Accidents in Nuclear Power Plants, Sorrento, Italy, March 1988.
[15] K.T. Kim, D.R. Olander, J. Nucl. Mater. 154 (1988) 85.
[16] P.J. Hayward, I.M. George, J. Nucl. Mater. 208 (1994) 35,43.
[17] M.S. Veshchunov, P. Hofmann, J. Nucl. Mater. 209 (1994) 27.
[18] M.S. Veshchunov, P. Hofmann, A.V. Berdyshev, J. Nucl. Mater. 231 (1996) 1.
[19] P. Hofmann, M. Markiewicz, J. Nucl. Mater. 209 (1994) 92.
[20] M.S. Veshchunov, P. Hofmann, J. Nucl. Mater. 228 (1996) 318.
[21] P. Hofmann, M. Markiewicz, Chemical interactions between as-received and pre-oxidized Zircaloy and stainless steel at high temperatures, Kernforschungszentrum Karlsruhe KfK-5106, 1994.
[22] P. Hofmann, M. Markiewicz, Chemical interactions between as-received and pre-oxidized Zircaloy and Inconel 718 at high temperatures, Kernforschungszentrum Karlsruhe KfK-4729, 1994.
[23] P. Hofmann, M. Markiewiez, J. Spino, Nucl. Technol. 90 (1990) 226.
[24] M. Veshchunov, P. Hofmann, J. Nucl. Mater. 210 (1994) 11.
[25] M. Veshchunov, P. Hofmann, J. Nucl. Mater. 226 (1995) 72.
[26] V. Noack, S. Hagen, P. Hofmann, G. Schanz, L. Sepold, Nucl. Technol. 117 (1997) 158.
[27] G. Bandini et al., Molten material relocation into the lower plenum: A status report, OECD/NEA Report (1997), NEA/CSNI/R (97) 34 (1998).
[28] T. Haste, B. Adroguer, N. Aksan, C. Allison, S. Hagen, P. Hofmann, V. Noack, Degraded core quench: A status report, OECD/NEA/CSNI/R (96) 14 (1996).
[29] P. Hofmann, V. Noack, M. Veshchunov et al, Physicochemical behavior of Zircaloy fuel rod cladding tubes during LWR severe accident reflood, Forschungszentrum Karlsruhe FZKA-5846, 1997.
[30] S. Hagen, P. Hofmann, V. Noack, L. Sepold, G. Schanz, Comparison of the quench experiments CORA-12, CORA-13 and CORA-17, Forschungszentrum Karlsruhe FZKA-5679, 1996.
[31] A.W. Cronenberg, Nucl. Technol. 97 (1992) 97.
[32] W. Hering, P. Hofmann, Material interactions during severe LWR accidents: Summary of separate-effects test

results, Kernforschungszentrum Karlsruhe KfK-5125, 1994.

[33] H. Kleykamp, R. Pejsa, Chemical and X-ray diffraction analysis on selected samples from the TMI-2 reactor core, Kernforschungszentrum Karlsruhe KfK-4872, 1991.

[34] S. Hagen, P. Hofmann, V. Noack, L. Sepold, G. Schanz, G. Schumacher, Cold lower end test CORA-10; Test results, Forschungszentrum Karlsruhe FZKA-5572, 1997.

[35] S. Hagen, P. Hofmann, V. Noack, L. Sepold, G. Schanz, G. Schumacher, Behavior of a VVER-1000 fuel element tested under severe accident conditions in the CORA Facility; Kernforschungszentrum Karlsruhe KfK-5212, 1994.

[36] S. Hagen, P. Hofmann, V. Noack, L. Sepold, G. Schanz, G. Schumacher, Behavior of a VVER-1000 fuel element with B_4C absorber tested under severe fuel damage conditions, Kernforschungszentrum Karlsruhe KfK-5363, 1994.

[37] S.S. Abalin, V.G. Asmolov, V.D. Daragan, E.K. D'Yakov, A.V. Merzliakov, V. Yu. Vishnevsky, in: Proceedings of the 8th International Topical Meeting on Nuclear Reactor Thermal-Hydraulics, Atomic Energy Soc. of Japan and the American Nuclear Soc. (ANS), Kyoto, Japan. vol. 2, 1997, pp. 581–586.

[38] P. Hofmann et al., Results of the commissioning tests in the QUENCH Facility, Forschungszentrum Karlsruhe FZKA-6099, 1998.

[39] P. Hofmann et al., QUENCH-01, Experimental and calculational results, Forschungszentrum Karlsruhe FZKA-6100, 1998.

[40] Proceedings of the Euratom Research Framework programme 1994–1998 Nuclear Fission Safety, FISA-97 Symposium on European Union research on severe accidents, Luxembourg, 17–19 November 1997, European Union Report EUR-18258 EN, 1998.